A Model for Predicting the Austenite Grain Size at the Surface of Continuously-Cast Slabs

CHRISTIAN BERNHARD, JÜRGEN REITER, and HUBERT PRESSLINGER

During the continuous-casting process, retarded cooling of the strand surface below oscillation marks and surface depressions results in the formation of coarse austenite grains. These coarse grains have proven to dramatically reduce the ductility of steel within the second ductility trough, and thus increase the risk of surface crack formation. In addition to the thermal history the composition of the steel, in particular the content of carbon and precipitation-forming elements, plays a decisive role in the development of the austenite grain size. The present work addresses the development and validation of an experimental and numerical model for predicting the austenite grain size in the continuous-casting process. In a first step, the previous austenite grain size on the surface of slabs was determined by metallographic examinations for several slabs with various carbon content. Next, a solidification experiment was adjusted in order to simulate the cooling conditions in the mold of a slab caster, but also to suppress the precipitation of nitrides and carbo-nitrides by subsequent accelerated cooling. Thus, it was possible to study the influence of steel composition on austenite grain growth at temperatures close to the solidus temperature, unaffected by precipitates. The results of both the plant and laboratory experiments point to a maximum austenite grain size with a carbon content of approximately 0.17 mass pct.

The parameters of a grain size prediction model were fitted to the results of the experiment. The resultant model was coupled with a precipitation model and then applied to the slab casting process. The measured and calculated grain size values at the surface and immediately below the surface of the slabs agree very closely. The model was finally applied to calculate the grain growth in the center of a virtual oscillation mark under simplified assumptions. Although only the surface temperature in the mold diverges significantly from the original solution, the difference of the initial cooling conditions results in an increase of the final grain size by up to 40 pct.

DOI: 10.1007/s11663-008-9197-8

I. INTRODUCTION

THE formation of transverse surface cracks has been a vital topic since the very early days of continuous casting. Reviews on the numerous publications can be found in references.[1–3] Based on the differentiation between a first and second brittle temperature range for steels at elevated temperature, the formation of transverse cracks is commonly attributed to an overcritical deformation in the second ductility trough. The second ductility trough is caused by the formation of precipitates, phases, or segregates along austenite grain boundaries. In addition to some alloying and microalloying elements, process related factors, such as deep oscillation marks or surface depressions[4–6] on the strand surface associated with coarse austenite grain size[7,8] also worsen crack susceptibility.

CHRISTIAN BERNHARD, Associate Professor, and JÜRGEN REITER, Research Associate, are with the Christian Doppler Laboratory of Metallurgical Fundamentals of Continuous Casting Processes, University of Leoben, 8700 Leoben, Austria. Contact e-mail: Christian.Bernhard@mu-leoben.at HUBERT PRESSLINGER, Senior Engineer, is with voestalpine Stahl GmbH, 4031 Linz, Austria.

Manuscript submitted October 9, 2006.
Article published online November 26, 2008.

The formation of transverse cracks may, however, also result from the formation of subsurface internal cracks below oscillation marks in or immediately below the mold, and the further propagation of the crack to the surface in the secondary cooling zone or during straightening.[9,10] This mechanism is not yet fully understood; the development of a laboratory simulation experiment is the aim of ongoing research.[11]

The conventional method for the characterization of the hot ductility of steel is the determination of the reduction of area (RA, pct) from hot tensile tests. A low RA indicates a higher crack susceptibility of the tested steel grade at the testing temperature. Depending on the testing conditions, a RA of more than 40 pct indicates a low crack susceptibility.[3] However, the definition of a clear deformation limit in order to prevent crack formation is rather difficult. The RA can be converted to strain-to-fracture or the critical strain ε_c by

$$\varepsilon_c = \ln\left(\frac{100}{100 - \mathrm{RA}}\right) \quad [1]$$

Assuming a critical RA of 40 pct, and inserting this value in Eq. [1] results in a calculated critical strain of

more than 50 pct. This is an unrealistic limit, since the total surface strain will not exceed 5 pct under common continuous-casting conditions.[6] Tensile tests on notched specimen in order to simulate the effect of oscillation marks yield a critical strain that falls below 10 pct depending on steel composition, the thermal cycle before testing, and the depth of the notch.[4–6] Transverse cracks will therefore most probably form on the bottom of deep oscillation marks and surface depressions.

Besides the notch effect and the associated stress concentration on the bottom of the oscillation mark, the reduced heat transfer in this area will result in the formation of coarse austenite grains. An increasing austenite grain size has a remarkable influence on the ductility in the second ductility trough, since the specific grain boundary area decreases while the precipitate density increases.[12] Cracks may also propagate easier by fewer sliding triple points[3] and the critical strain for the onset of dynamic recrystallization increases.[13,14] According to Mintz *et al.*,[3] the minimum RA in the second ductility trough is reciprocal to the square root of the austenite grain diameter with decreasing influence of grain diameters above 300 μm. Other authors, like Ohmori and Kunitake,[15] found the elongation to be reciprocal to the grain diameter for grain diameters above 100 μm.

Since the fundamental work of Yasumoto *et al.* and Maehara *et al.*[4,16,17] the main influencing parameters on austenite grain growth are known: steel composition, the starting temperature for austenite grain growth, and the cooling rate during and after solidification. For cooling rates between 0.1 °C/s and 1.5 °C/s, Miettinen[18] fitted the experimental results of Yasumoto *et al.*[17] using the following equation:

$$\bar{D} = 21 \cdot T^{\gamma} - 3152 \cdot \left[\frac{e^{\dot{T}}}{1 + e^{\dot{T}}} \right] - 25,088 \qquad [2]$$

In Eq. [2], T^{γ} denotes the highest temperature of a totally austenitic structure in °C, $\dot{T}$ is the local cooling rate of solidification in °C/s, and $\bar{D}$ is the final austenite grain size in μm. The influence of precipitation is neglected. Under similar cooling conditions, the maximum grain size is thus found for a carbon equivalent of 0.17 mass pct, due to the highest temperature for a totally austenitic structure in the Fe-C system.

Further data for austenite grain growth after solidification was derived in *in-situ* hot tensile tests by Deprez *et al.*[5] This work underlines the importance of melting the probe before cooling it down to the testing temperature. This thermal cycle results in coarse austenite grain, especially for steels with 0.15 and 0.2 mass pct C, and a clearly lower RA in the ductility trough.

Schwerdtfeger *et al.*[19] addressed a combined experimental and numerical simulation of austenite grain growth. The numerical approach couples a grain growth model proposed by Andersen and Grong[20] with an Nb(C,N)-precipitation model,[21] in regard to the influence of deformation-induced precipitation. The maximum grain size is found for 0.17 mass pct C. The grain growth model is coupled with a thermal model in order to calculate grain growth under continuous-casting conditions.

A recent work addresses the measurement of austenite grain size on the surface of continuously-cast slabs for typical high-strength structural steels.[22] Typical average values range from 400 to 800 μm at the surface and from 600 to 1600 μm at the center of oscillation marks (0.16 to 0.20 mass pct C steels).

The previous overview on literature focused on regular grain growth, the influence of steel composition, and the increase of the grain size by a reduced cooling rate, *e.g.*, in the center of oscillation marks. Besides the regular grain growth, also abnormally large prior-austenite grains may lead to the formation of surface defects on the cast semi or in the subsequently rolled product, as referred to in a recent publication by Dippenaar *et al.*[23] The formation of these "blown grains" with a diameter of up to several millimeters is described as a mostly local phenomenon and attributed to a high surface temperature and strain. The background behind the abnormal grain growth is not yet fully understood. The consequence for the surface quality of the product is in any way dramatic.

The general view of the influence of steel composition on the austenite grain size is uniform; under similar cooling conditions, a maximum has to be expected for a carbon equivalent of around 0.17 mass pct, associated with a minimum in ductility within the second ductility trough. Precipitates are assumed to drag the grain growth depending on volume fraction and radius of particles and thus, depending on the content in precipitation-forming elements, the grade and rate of deformation and the thermal history. However, precipitations do not play as much of an important role for the austenite grain growth in continuous casting as in the subsequent reheating/rolling process. In continuous casting, even the surface of a slab remains above the temperature for nitride and carbo-nitride precipitation for a relatively long time. During this period, the driving force for grain growth is high, and the austenite grains rapidly achieve diameters of several hundred microns. These large grains grow much slower, additionally retarded by the decreasing temperature and thus, the decreasing driving force for grain growth. At typical AlN equilibrium precipitation temperatures around 1100 °C the growth rate is already low and the influence of the precipitations on the final austenite grain size is small. In microalloyed steels, (Ti,Nb)(C,N) precipitates form at higher temperature and may therefore be of greater importance.

The present work first addresses the measurement of austenite grain size in the near-surface region of slabs with a carbon content between 0.15 and 0.53 mass pct, cast at caster 5 of voestalpine Stahl in Linz. The measured data serves as a benchmark for the development of a laboratory simulation experiment and the final validation of a numerical grain size prediction model. The laboratory experiment allows the simulation of the initial solidification under slab casting conditions and the prevention of the precipitation of nitrides and carbo-nitrides during subsequent cooling. The apparent

activation energy for grain growth was determined from the results of the experiment, assuming a linear dependency on carbon content. The grain size prediction model was finally coupled with a precipitation model and used to calculate the austenite grain size at the surface of continuously-cast slabs. The comparison of the calculated and measured values points to the validity of the model over a wide range of steel compositions.

II. GRAIN SIZE MEASUREMENT ON CONTINUOUSLY-CAST SLABS

A set of eight slabs was selected for the metallographic examination, for composition and measured grain diameter see Table I. The equivalent carbon content c_p is calculated using a simplified form of the formula proposed by Howe:[24]

$$c_p = \text{mass pct C} - 0.14 \cdot \text{mass pct Si} + 0.04 \cdot \text{mass pct Mn} \quad [3]$$

Slabs A, B, C, D, and F were cast at a casting speed of 1.2 m/min, slab E with 1 m/min, and slabs G and H with 0.9 m/min. Slabs G and H were cast with a thickness of 285 mm, and slabs A through F with 215 mm.

For every slab, an 18×70 mm^2 area, parallel to the surface and 400 mm off the corner, was ground, polished, and etched. In order to not only derive the mean grain size, but also the grain size distribution, the selected grain size measurement method differs from the methods described in the well-known standards (ASTM E112 or DIN EN ISO 643). A number of at least 200 grains was marked by hand on every micrograph in a digital image analysis system. The number and area of the grains was then automatically determined. The parameters for the statistic distribution as well as the average value were finally calculated by statistics software. This procedure was repeated in steps of 10 mm, starting from the surface and ending in the middle of the slab, or in a position where the austenite grain size could no longer be detected.

Figure 1 shows as an example two micrographs with prior-austenite grains in a distance of 10 and 90 mm from the slab surface for slab A. In order improve the contrast, the pro-eutectoid cementite along the prior-austenite grains has been additionally highlighted. The coarsening of the grains with increasing distance from the surface is clearly visible and the average grain diameter amounts to 1.78 and 3.24 mm, respectively.

Development of a suitable etching technique in order to reveal the former austenite grain boundaries turned out to be a complex problem. It was not possible to reveal the structure at the surface of steels with less then

Table I. Chemical Composition of Steels and the Measured Mean Grain Diameter

	Steel Composition, in Mass Pct								Mean Grain Diameter (mm)	
Slab	C	Si	Mn	Al	Nb	Ti	N	c_p	$\bar{D}_0$	$\bar{D}_{10}$
A	0.168	0.21	1.50	0.032	0.001	0.002	0.0033	0.20	0.98	1.78
B	0.185	0.22	0.69	0.036	0.001	0.002	0.0080	0.18	0.71	1.65
C	0.530	0.24	0.86	0.042	0.002	0.005	0.0050	0.53	0.58	0.66
D	0.210	0.22	1.45	0.047	0.001	0.003	0.0036	0.24	0.84	1.52
E	0.152	0.02	1.09	0.039	0.001	0.001	0.0070	0.19	—	1.49
F	0.210	0.19	1.54	0.048	0.003	0.002	0.0060	0.25	—	1.57
G	0.171	0.44	1.54	0.039	0.022	0.004	0.0038	0.17	0.59	1.79
H	0.174	0.16	1.47	0.031	0.028	0.001	0.0028	0.21	—	1.76

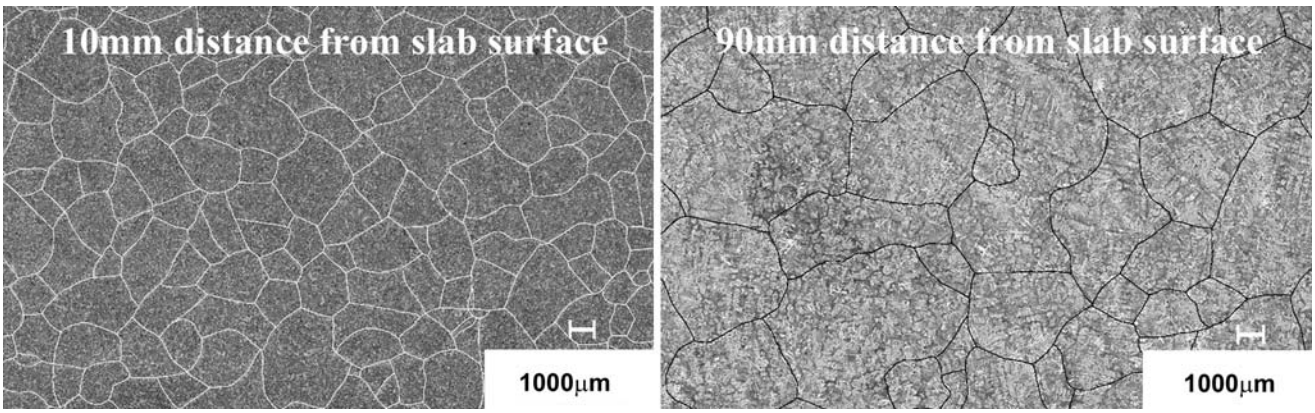

Fig. 1—Austenite grain size at two different distances from the slab surface for slab A with 0.17 mass pct C (etchant: ammonium persulfate) with traced grains.

0.1 mass pct carbon and also for the slabs E, F, and H clearly enough to measure more than 200 grains. The respective values are therefore not displayed in Table I. The results of the etching experiments and the grain size measurement method will be described in detail in a separate publication.[25] Assuming round grains, the diameter of the grain is calculated from the mean grain area, A, with $D = 2 \cdot \sqrt{A/\pi}$. Table I gives the mean grain diameter at the surface $\bar{D}_0$ and in a distance of 10 mm below the surface $\bar{D}_{10}$.

Figure 2 gives an example of the grain size distribution near the surface for slabs A and C. The measured grain size fits with a lognormal distribution.[26] The average grain diameter $\bar{D}_0$ is 0.98 mm for steel A and 0.58 mm for steel C. The average final grain size will be used for further correlations with the influencing variables on grain growth. The grain size distribution serves as an additional benchmark for the results of the laboratory experiment.

Figure 3 shows the average grain diameter *vs* equivalent carbon content. A maximum of the austenite grain size around 0.2 mass pct can be assumed, but the influence of the steel composition is superimposed by different cooling conditions, resulting from the grade-specific secondary cooling strategy. These uncertainties are the main reason for simulating the austenite grain growth under more controlled conditions in the laboratory scale. The development of this experiment will be discussed in detail in Section III.

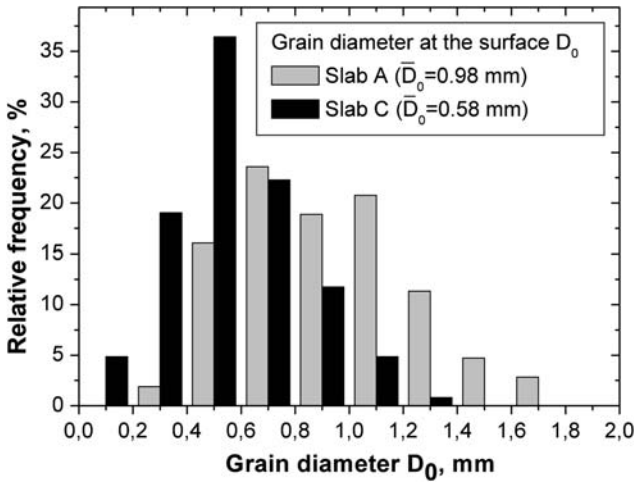

Fig. 2—Grain size distribution at the surface for slabs A and C.

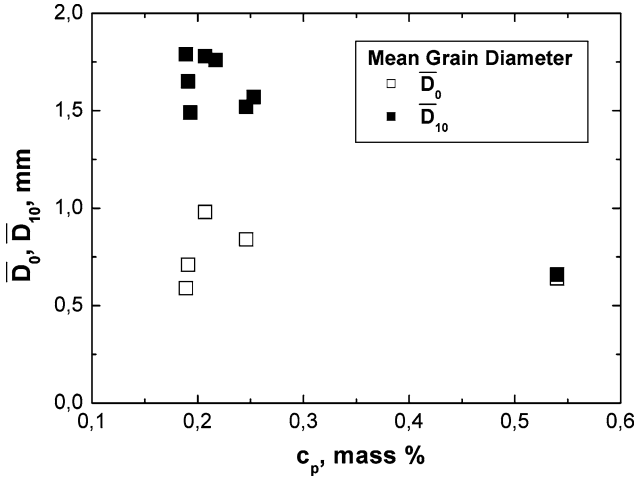

Fig. 3—Average grain diameter at the surface $\bar{D}_0$ and 10 mm below the surface. $\bar{D}_{10}$ *vs* equivalent carbon content c_p for slabs in Table I.

III. EXPERIMENTAL SIMULATION OF AUSTENITE GRAIN GROWTH UNDER CONTINUOUS-CASTING CONDITIONS

As mentioned previously, the steel composition and the thermal cycle are the most relevant parameters determining the austenite grain size in the continuous-casting process. The cooling of the strand surface in the slab casting process is characterized by a relatively high heat extraction in the mold, a recurrent change of contact with water sprays, rolls and atmosphere within the secondary cooling zone, and finally, the heat transfer through radiation during further cooling.

It was not the aim of the present experiment to reproduce the surface temperature along the whole length of the slab in the casting machine. In fact, only the initial solidification and subsequent cooling of the strand surface in the mold of a casting machine should have been simulated. The subsequent accelerated cooling of the specimen prevented the precipitation of nitrides at higher temperatures. The Submerged Split Chill Tensile (SSCT)-test principle[27–29] was adopted for the experiments. Thereby, a coated cylindrical steel substrate is submerged into liquid steel in an induction furnace. The liquid steel solidifies at the surface of the substrate. The thickness of the ceramic coating controls the heat transfer between the solidifying shell and the substrate. The microstructure of the shell is columnar and the characteristic microstructure parameters, primary and secondary dendrite spacing, correspond to those in a slab, bloom, or billet.[30]

After a dwell time of 30 seconds, shell and substrate are removed from the melt (Figure 4). The thickness of the shell amounts to between 12 and 14 mm at that time. After cooling in the atmosphere to room temperature, the solidified shell is cut into 16 pieces. Each of these pieces is prepared for metallographic examination and the austenite grain size is determined with the method described.

The accurate control of the thermal conditions during the test is an important prerequisite for the analysis of the results. For this purpose, two thermocouples are clamped at a specified distance from the surface of the substrate in order to measure the temperature increase. Another thermocouple is positioned inside the solidifying shell. The measured temperatures serve as input data for an inverse thermal model.[30] A typical calculated cooling curve for the shell at the interface with the substrate for cooling in air is shown in Figure 5. The precipitation of AlN at temperatures above 900 °C is unlikely, even for the highest Al content of all experiments (0.059 mass pct) and a nitrogen content of 0.006 mass pct.

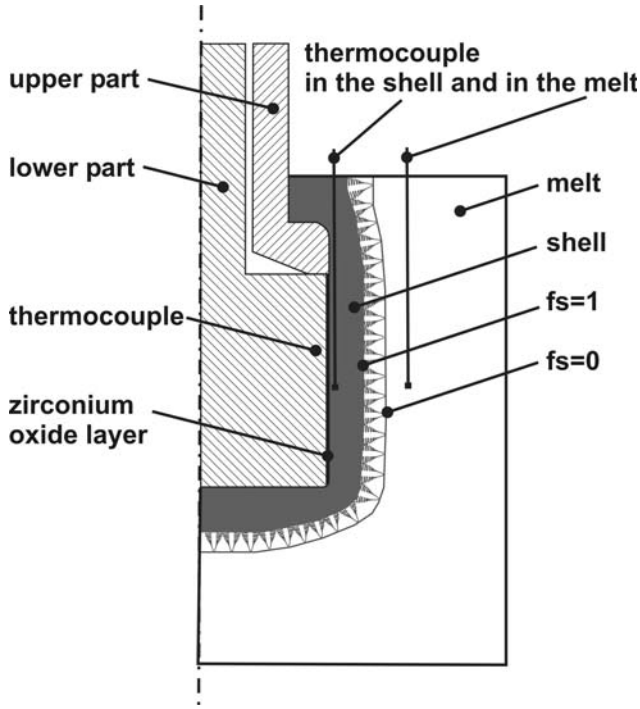

Fig. 4—Test body with thermocouples and solidifying shell.

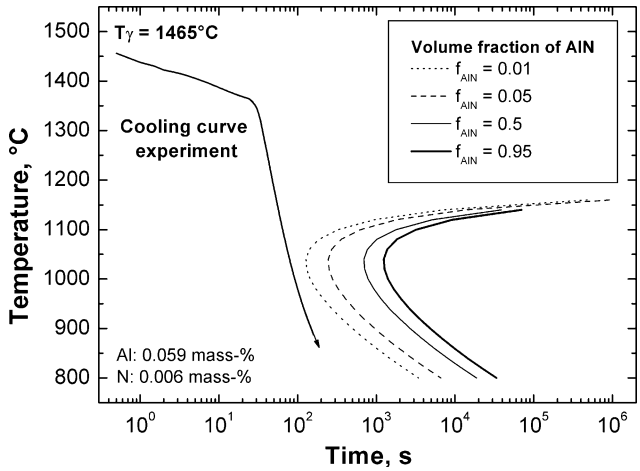

Fig. 5—Temperature of shell at interface with substrate as a function of time for the experiment with subsequent cooling in air and time-temperature-precipitation diagram for steel with 0.059 mass pct Al and 0.006 mass pct N.

The actual work presents the results of two tests series: the first with a carbon content of between 0.15 and 0.4 mass pct C and a Mn content with between 0.30 and 0.38 mass pct, and the second with between 0.05 and 0.70 mass pct C and between 1.04 and 1.88 mass pct Mn. The composition of these steels, combined with the calculated equivalent carbon content c_p and the measured mean grain diameter in 1-mm distance from the surface, $\bar{D}_1$ in mm, are given in Table II. This distance from the surface was selected for the austenite grain size measurement because it proved to be the closest distance to the surface, where 200 grains could be measured for all experiments. The control of the thermal conditions during the experiment is ensured by the thermal model and the measured temperature at 1-mm distance from the surface. The mechanism of grain growth is supposed to be the same as at the surface.

Table II. Chemical Composition, Measured Grain Diameter, and T^{γ} for the Experiments

Test	C (Mass Pct)	Si (Mass Pct)	Mn (Mass Pct)	c_p (Mass Pct)	$\bar{D}_1$ (mm)	T^{γ} (°C)
A1	0.15	0.21	0.31	0.13	1.29	1470
A2	0.15	0.21	0.30	0.13	1.31	1460
A3	0.45	0.18	0.30	0.44	0.54	1416
A4	0.37	0.19	0.38	0.36	0.55	1433
A5	0.40	0.19	0.32	0.39	0.64	1428
B1	0.05	0.25	1.44	0.07	0.68	1432
B2	0.10	0.26	1.46	0.12	0.99	1453
B3	0.20	0.26	1.45	0.22	0.80	1452
B4	0.51	0.27	1.45	0.53	0.44	1391
B5	0.15	0.21	1.04	0.16	1.29	1468
B6	0.16	0.22	1.88	0.20	0.99	1434
B7	0.08	0.30	1.36	0.09	1.03	1474
B8	0.12	0.28	1.34	0.13	1.11	1460
B9	0.51	0.29	1.28	0.52	0.40	1391
B10	0.70	0.25	1.34	0.72	0.38	1358

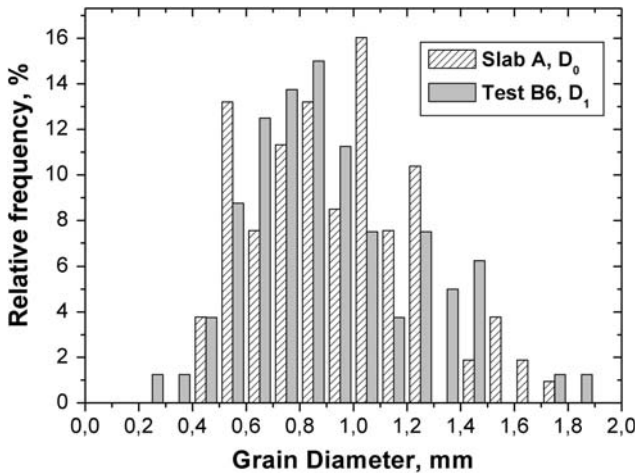

Fig. 6—Grain size distribution at surface of slab A compared with grain size distribution in 1-mm distance from the surface for test B6, both with an equivalent carbon content of 0.21 mass pct.

The target Al content was 0.03 mass pct for all experiments, the highest Al content is 0.059 mass pct. The N content is typically 0.006 mass pct and T^{γ} denotes the highest temperature of a totally austenitic structure in degrees Celsius, calculated using the software package InterDendritic Solidification (IDS, TKK Laboratory of Metallurgy, Helsinki University of Technology, Espoo, Finland). Figure 6 compares the grain size distribution at the surface of slab D with the grain size distribution 1 mm below the surface for test B6. For both steels c_p is 0.21 mass pct. The good correlation of the characteristic of the grain size distribution is evident. The perfect coincidence of the average grain size,

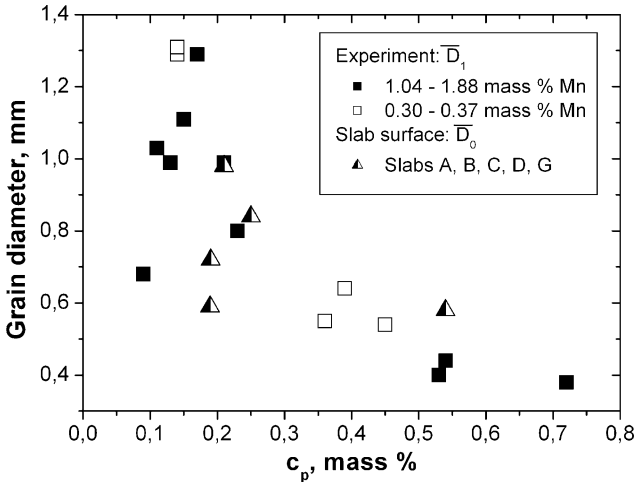

Fig. 7—Average grain size $\bar{D}_0$ for all slabs and $\bar{D}_1$ for all laboratory tests *vs* equivalent carbon content.

0.99 mm for B6 ($\bar{D}_1$) and 0.98 mm for slab A ($\bar{D}_0$), might be capable of being misunderstood. It is not the aim of the experiment to simulate the final austenite grain size at the surface of a slab, however different cooling cycles together with pinning effects of particles in continuous casting might result in the same final grain size.

Figure 7 illustrates the influence of the equivalent carbon content on $\bar{D}_1$ for all tests. The results show the expected maximum between a c_p of 0.15 and 0.17 mass pct. The influence of the steel composition is remarkable; under identical cooling conditions, the final average austenite grain diameter varies by a factor of more than 3. The influence of Mn on the grain size seems to be well explained by its consideration in the calculation of the equivalent carbon content. The measured values are in a similar range as the measured grain size on the slab surface.

IV. GRAIN SIZE PREDICTION MODEL

Andersen and Grong[20] proposed the following simple differential equation, which describes the variation in the average grain size $\bar{D}$ with time t and temperature T (in Kelvin) in the presence of pinning precipitates:

$$\frac{d\bar{D}}{dt} = M_0^* \cdot e^{\left(-\frac{Q_{app}}{R \cdot T}\right)} \cdot \left(\frac{1}{\bar{D}} - \frac{1}{k} \cdot q_p\right)^{\left(\frac{1}{n}-1\right)} \quad [4]$$

In this formula, M_0^* denotes a kinetic constant that describes the grain boundary mobility in $m^2\ s^{-1}$, Q_{app} is the apparent activation energy for grain growth in J/mol, and R is the gas constant (8.3145 J/mol K). The driving force for grain growth is reciprocal to the actual grain diameter $\bar{D}$. This driving force is counteracted by a pinning force, exerted by precipitations on the boundary. The term $\frac{k}{q_p}$ represents the maximum grain diameter under normal grain growth conditions, the so-called Zener limit.[31] The calculation of q_p will be described in the subsequent section. The time exponent n is a measure of the resistance to grain boundary motion in the presence of impurities and alloying elements in solution.[20] According to an analysis of grain growth data, n is always less than or at most equal to 0.5.[32]

The present experiments were all performed under similar cooling conditions and were not interrupted after a specified time to investigate the time development of the grain size. Thus, the results give only information about the final grain size and not about grain growth. Some initial values for the parameters in Eq. [4] were therefore determined from the analysis of grain growth experiments on two plain carbon steels.[33] The M_0^* was assumed with $4 \cdot 10^{-3}\ m^2\ s^{-1}$[19] and Q_{app} and q_p were used as fitting parameters; Q_{app} as a steel grade specific constant, and q_p as dependant on temperature and steel grade but constant in time. The effect of precipitation or dissolution kinetics was thus neglected. Under these assumptions, a sufficient correspondence of the characteristic of the measured and calculated grain size resulted for a constant and steel grade independent time exponent of 0.5.

For a 0.17 mass pct C, Al-killed plain carbon steel, and holding temperatures of between 1050 °C and 1150 °C, Q_{app} was determined with 180.2 kJ/mol. For a 0.78 mass pct carbon steel and holding temperatures of between 1000 °C and 1100 °C, the best fit for Q_{app} is 208.8 kJ/mol. A decreasing driving force for grain boundary movement with increasing carbon content was also found by other authors.[34]

Adopting the time exponent 0.5 and disregarding the influence of precipitates leads to the following simplified form of Eq. [4]:

$$\frac{d\bar{D}}{dt} = M_0^* \cdot e^{\left(\frac{-Q_{app}}{RT}\right)} \cdot \left(\frac{1}{\bar{D}}\right) \quad [5]$$

As the local temperature during the solidification experiment is not a simple time-dependant function, Eq. [5] has to be solved numerically for the calculated temperature evolution displayed in Figure 6:

$$\bar{D}(t + \Delta t) = \bar{D}(t) + M_0^* \cdot e^{\left(\frac{-2Q_{app}}{R(T_i + T_{i+1})}\right)} \cdot \left(\frac{1}{\bar{D}(t)}\right) \cdot \Delta t \quad [6]$$

For the analysis of the experimental results, the final mean grain size is compared with the measured grain size. The activation energy Q_{app} serves as fitting parameter. The initial grain size is in the range of a primary dendrite arm spacing,[35] for the present experiment constant 100 μm. The highest temperature for a totally austenitic structure T^{γ} is used as the start temperature for grain growth (Table II). The calculation procedure is stopped when the temperature falls below the Ar_3 temperature.

Figure 8 presents the calculated Q_{app} values *vs* carbon content for the steels in Table II, together with the Q_{app} values from the analysis of the isothermal grain growth experiments. Assuming a linear increase of Q_{app} with the carbon content results in the following empirical relationship (for C > 0.1 mass pct):

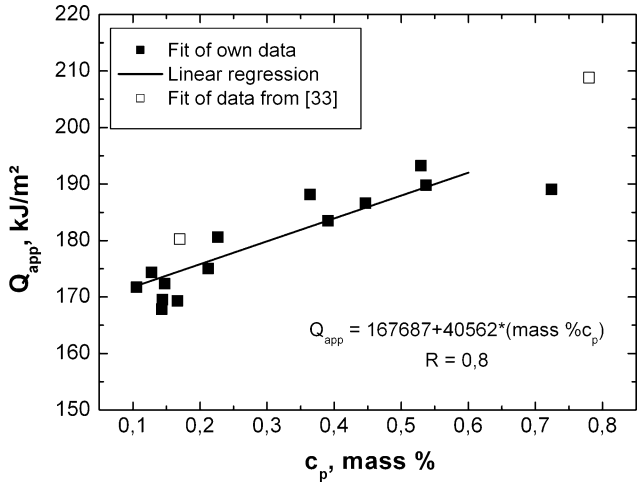

Fig. 8—Apparent activation energy for grain growth *vs* carbon content for all experiments with linear regression.

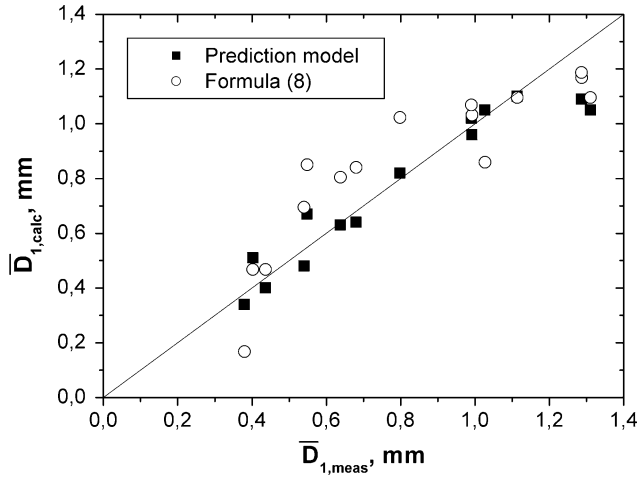

Fig. 9—Austenite grain size from prediction model (Eq. [6]) and Eq. [8] *vs* measured average austenite grain size for laboratory tests.

$$Q_{\text{app}} = 167,686 + 40,562 \cdot (\text{mass pct } c_p) \qquad [7]$$

The calculated *vs* measured austenite grain size is plotted in Figure 9 using full symbols for the steels in Table II. The correspondence over a wide range of carbon contents is apparent. Only the highest grain size values seem to be underestimated in evidence.

Taking the approach from Eq. [2], assuming the initial cooling rate to be 10 °C/s and fitting the first and last constant to the measured results yields the following equation:

$$\bar{D} = 9.1 \cdot T^{\gamma} - 3152 \cdot \left[\frac{e^{\dot{T}}}{1 + e^{\dot{T}}} \right] - 9044 \qquad [8]$$

The resultant final austenite grain size is plotted in open symbols in Figure 9. It can be seen that the predicted and measured values also closely agree. The difference between the original constants and the newly fitted values might be attributed to the different experimental conditions; the original values were valid for cooling rates between 0.5 °C/s and 1.5 °C/s, which is quite far below the cooling rates in this experiment. However, the deviation points also to an underestimation of the influence of the cooling rate on the final grain size. The validity of Eq. [8] is therefore limited to initial cooling rates of around 10 °C/s.

V. PRECIPITATION CALCULATIONS

As already pointed out, the pinning effect of precipitates was deliberately minimized during the solidification experiment by relatively high cooling rates. This afforded the advantage that the activation energy was determined without uncertainties about the accuracy of the calculation of particle fractions and particle radii. By the same token, however, the relevance of this simplified model for continuous-casting conditions appears limited. Therefore, a precipitation model was coupled with the austenite grain growth model.

The term $\frac{1}{k} \cdot q_p$ in Eq. [4] includes the retardation of grain growth by particles. The Zener coefficient k describes the pinning efficiency of the precipitates and is, according to the original Zener model, assumed to be 4/3.[31] According to Eq. [9], q_p, the pinning force parameter in m^{-1}, represents the fraction f/r integrated over all classes of precipitates, where f is the volume fraction and r the radius of the precipitates.[19] The volume fraction of every class of particles is the number of particles N, nucleated at time τ, times the actual volume of the particles nucleated at time τ, per volume of the system. The actual radius of the particles nucleated at time τ is $r(t, \tau)$.

$$q_p(t) = \frac{f}{r} = \int_0^t \frac{f(t,\tau)}{r(t,\tau)} d\tau \qquad [9]$$

Overall, the actual procedure for the calculation of q_p follows the method applied by Schwerdtfeger *et al.*,[19] except that besides Nb(C,N) precipitates, AlN precipitations are also considered and that deformation induced precipitations are disregarded.

According to the precipitation reaction of AlN,

$$[\text{Al}] + [\text{N}] \leftrightarrow (\text{AlN}) \qquad [10]$$

the free energy of formation, ΔG_{AlN} in J/mol, is given by

$$\Delta G_{\text{AlN}} = \Delta G_{0,\text{AlN}} - \text{R} \cdot T \cdot \ln K_{\text{AlN},\gamma} \qquad [11]$$

with R being the gas constant (8.3145 J/mol K) and an equilibrium solubility product of AlN in austenitic iron of[36]

$$\log K_{\text{AlN},\gamma} = \log[\text{pct Al}] \cdot [\text{pct N}] = -\frac{6770}{T} + 1.03 \qquad [12]$$

and the standard Gibbs energy of formation $\Delta G_{0,\text{AlN}}$ in J/mol,[35]

$$\Delta G_{0,\text{AlN}} = -129,610 + 19.72 \cdot T \qquad [13]$$

The free energy of nucleation is given by

$$\Delta G_{\text{crit}} = \frac{16\pi}{3} \cdot \frac{\sigma^3}{\Delta G_{\text{AlN}}^2} \cdot V_{\text{AlN}}^2 \qquad [14]$$

where σ, the specific interface energy between the matrix and the AlN precipitate, is assumed to be 0.2 J/m^2.[37] The molar volume of austenite V_{AlN} is $1.26 \cdot 10^{-5}$ m^3·mol^{-1}.[19]

Under the assumption of thermodynamic equilibrium at the interface between steel and particle and in consideration of the fact that the diffusion coefficient of Al is much smaller compared to the one of N, the growth of a particle with radius $r(t)$ (in meters) during Δt can be calculated by

$$r(t+\Delta t) = \sqrt{r(t)^2 + 2D_{\text{Al}} \cdot \left(\frac{[\text{pct Al}]_{(t)} - [\text{pct Al}]_e}{\frac{100 \cdot M_{\text{Al}}}{\rho_{\text{Fe}} \cdot V_\gamma} - [\text{pct Al}]_e} \right) \cdot \Delta t} \qquad [15]$$

In Eq. [15], $[\text{pct Al}]_{(t)}$ denotes the actual Al concentration in the matrix. The effective diffusion coefficient of Al in austenite is given by

$$D_{\text{Al}}(T) = D_{0,\text{Al}} \cdot e^{\frac{-Q_{D,\text{Al}}}{R \cdot T}} \qquad [16]$$

with $D_{0,\text{Al}}$ being $1.8 \cdot 10^{-4}$ m^2·s^{-1} and $Q_{D,\text{Al}}$ being 228,200 J/mol.[37] The equilibrium Al concentration at the interface between the matrix and precipitate is calculated using

$$[\text{pct Al}]_e = \frac{K_{\text{AlN},\gamma}}{[\text{pct N}]_\infty} \qquad [17]$$

The nucleation rate per volume $\frac{dN(t)}{dt}$ is calculated from

$$\frac{dN(t)}{dt} = N_0 \cdot D_{\text{Al}}(T) \cdot [\text{pct Al}]_\infty \cdot e^{\frac{\Delta G_{\text{crit}}}{k_B \cdot T}} \qquad [18]$$

where N_0 denotes a factor that is proportional to the density of nucleation sites and where N_0 is commonly used as a fitting parameter in order to adjust the precipitation model to, for example, the results of hot tensile tests.[19,39] The present work assumes N_0 with $3.25 \cdot 10^{25}$ m^{-5}. The Boltzmann constant k_B is $1.38 \cdot 10^{-23}$ J/K.

The q_p is given by the particle volume fraction f divided by the radius $r(t,\tau)$. The particle volume fraction at time t, is then given by the sum of the actual volume of each particle, nucleated at time τ multiplied by the number of particles, nucleated at time τ:

$$q_p(t) = \frac{4\pi}{3} \cdot \sum_{\tau=0}^{\tau=t} r(t,\tau)^2 \cdot N(t,\tau) \qquad [19]$$

The prediction of the precipitation of Nb(C,N) follows the same procedure, all parameters were taken from Reference 19 without any adjustment. The total pinning force parameter is assumed to be the sum of the pinning force of the precipitated AlN and the precipitated Nb(C,N).

The precipitated volume fraction X is the ratio between the actual particle volume fraction and the particle volume fraction under assumption of thermodynamic equilibrium at the present temperature. Under isothermal conditions, X amounts to a value of less or equal 1 when the system is under equilibrium. Under continuous-casting conditions, the permanent temperature fluctuations at the strand surface may also result in a precipitated volume fraction that exceeds 1.

$$X = \frac{f(t)}{f_e(t)} \qquad [20]$$

Figure 10 shows an example of the application of the simple AlN-precipitation model to the continuous-casting process. On the basis of the typical calculated surface temperature for a slab casting machine (casting speed 1 m/min),[38] X was calculated, assuming a constant Al content of 0.047 mass pct (according to slab D) and varying the N content between 0.004 and 0.008 mass pct. The difference is remarkable; for the highest N content, X amounts to 0.3, whereas in the case of a low N content the precipitated fraction of AlN is one order of magnitude lower.

Figure 11 shows the resultant influence of the AlN precipitation on austenite grain growth, applying the model and parameters developed from the laboratory experiments. The grain growth is assumed to stop as soon as $3/4q_p$ exceeds the increment of the grain diameter, according to the Zener model. The time up to the total pinning of the grain boundaries is 18 minutes for steel with a low N content, corresponding to a final mean grain size of 0.72 mm. In the case of the 0.008 mass N steel, grain growth stops after only 5 minutes corresponding to a final austenite grain size of only 0.53 mm.

The previously described results have been calculated based on a cooling curve that is typical for low casting speed and relatively intensive secondary cooling. Under these conditions, the first few minutes or even fractions of a minute of cooling are decisive for the final grain size, since the grain boundary mobility is already very limited below the mold. If the surface temperature in the

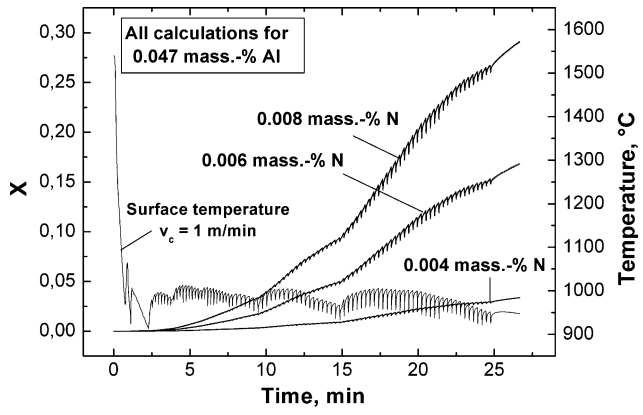

Fig. 10—Temperature on surface of a slab *vs* time in casting machine, combined with precipitated volume fraction of AlN for different N content.

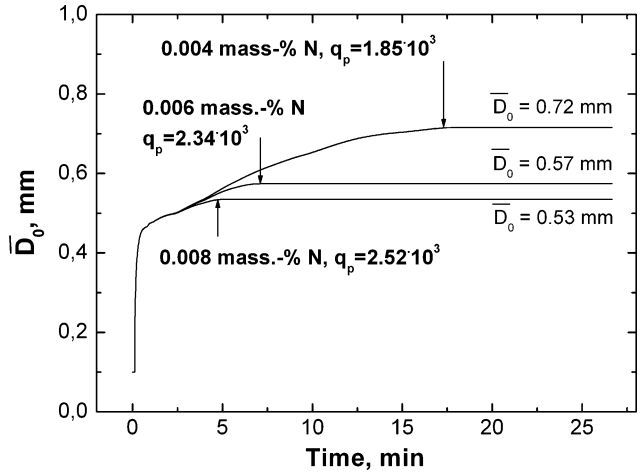

Fig. 11—Calculated austenite grain growth *vs* time for surface temperature in Figure 10 and influence of pinning particles on final grain size.

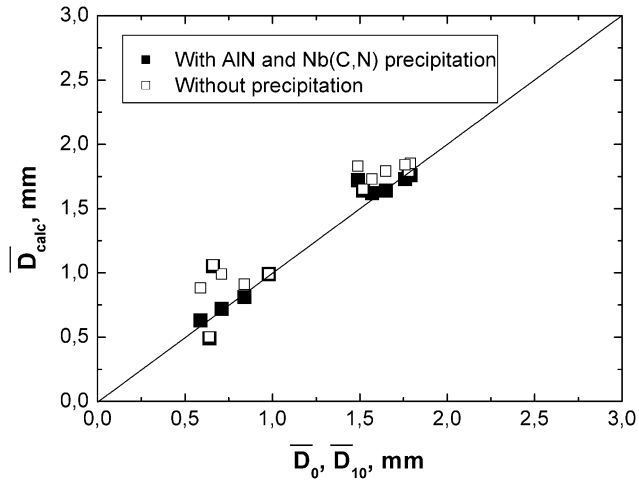

Fig. 12—Calculated austenite grain size *vs* measured grain size for experiments in Table I.

secondary cooling zone is generally on a higher level, which is possible for a higher casting speed or a reduced secondary cooling intensity, the grain boundary mobility also remains high. The grain growth will continue until the end of the secondary cooling zone or until the pinning effect of precipitations retards the grain growth. This depends on the content of nitride and carbo-nitride forming elements. Thus, the influence of precipitations on the final austenite grain size might be even more important.

VI. VALIDATION OF THE COUPLED AUSTENITE GRAIN SIZE PREDICTION MODEL

The parameters in the austenite grain growth model have been fitted to the results of the laboratory experiments, indicating the validity of the general assumptions. The validation of a precipitation model by experiments would be much more complex and go far beyond the scope of this work. The parameters in the precipitation model, namely, the factor N_0 in Eq. [18], were therefore adjusted in order to fit the results of precipitation models in other publications[39] or adopted from other publications.[19] The reliability of the results proved to be sufficient to represent the influence of pinning forces on the austenite grain growth under continuous-casting conditions.

The grain size prediction model was used finally to calculate the grain growth for the slabs in Table I and the results are summarized in Figure 12. The open symbols represent the results without taking precipitation into consideration. The good correspondence to the measured results is obvious. Nevertheless, the consideration of AlN and Nb(C,N) precipitation in the model permits further improvement, particularly at the surface. In increasing distances from the surface, the volume elements remain at temperatures above the precipitation temperature for a longer time. The grains achieve large diameters and therefore already grow very slow, before precipitations retard the grain growth.

The initial cooling of the surface in the mold is comparably higher. During the subsequent secondary cooling, it is meaningful to hold the surface temperature as long as possible above the precipitation temperature in order to go out of the second ductility trough, and thus to prevent the formation of surface cracks. Therefore, the decrease in the prior-austenite grain size at the surface caused by the retardation of grain growth due to precipitations is also rather low (<30 pct). However, it seems necessary to note that any variation of the cooling strategy or the casting speed might completely change the situation and make the nitride and carbo-nitride precipitations an important factor for the final austenite grain size.

The retarded local cooling of the strand surface on the bottom of an oscillation mark is an illustrative example of the influence of the initial cooling conditions on the final austenite grain size. The calculation of the surface temperature on the bottom of an oscillation mark is based on the assumption of reduced local heat flux in the mold. According to literature, a reduction of the heat flux by between 20 and 30 pct seems realistic, depending on the depth of the oscillation mark.[40] The heat transfer in the secondary cooling zone remains unmodified. Significant changes in the surface temperature can therefore only be observed in the mold, which can be seen in Figure 13, for the example from Figure 9 and a reduced heat flux in the mold q_m by 20 and 30 pct, respectively. The influence of the marginal temperature differences is remarkable. The final austenite grain size increases from 0.72 to 0.93 and 1.03 mm. This ratio between the grain size in the middle of oscillation marks and the surrounding area amounts to 40 pct and more, which would agree very well with the results of metallographic examinations on slab surfaces.[22]

VII. CONCLUSIONS

The present work deals with measurement of austenite grain size on slabs and specimens from laboratory

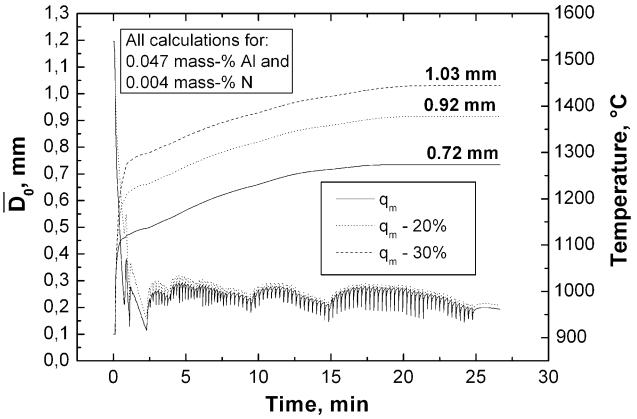

Fig. 13—Strand surface temperature for a reduced heat flux in the mold and simultaneous austenite grain growth with final average grain size.

experiments, as well as the adjustment of parameters in a grain size prediction model for the continuous-casting process.

The measured austenite grain size and grain size distribution on the surface of slabs was the basis for the development of a solidification experiment. This experiment allows the laboratory simulation of initial solidification under conditions close to the continuous-casting process, but restrained precipitation of nitrides and carbo-nitrides. The apparent activation energy for grain growth Q_{app} served as fitting parameter in order to adjust the measured grain size to the results of the experiments. The following correlation between Q_{app} and the carbon content within the range of the steel composition in the experiment (0.05 to 0.70 mass pct C) was derived:

$$Q_{app} = 167,686 + 40,562 \cdot (\text{mass pct C})$$

The grain size prediction model allows an accurate description of the experimental results. A clear maximum of the final grain size was found for an equivalent carbon content of between 0.15 and 0.17 mass pct, according to the results of other authors.[4,5,19]

In order to apply the model to the continuous-casting process, the consideration of retardation of grain growth by pinning forces seemed to be essential. Therefore, an AlN and Nb(C,N)-precipitation model from literature[19] was implemented into the grain growth model. The simulation of grain growth at the strand surface and the subsequent comparison of calculated and measured average grain size proved the validity of the model over a wide range of steel compositions. Thereby, the influence of precipitates on the final grain size depends on the surface temperature and the content in microalloying elements. Under the given process conditions and steel compositions, precipitates reduce the final austenite grain size by between 1 and 30 pct. Considering the uncertainties in the measurement of the austenite grain size, these differences seem marginal. In any case, the consideration of pinning forces improves the results and for higher casting speed or soft cooling conditions with a generally higher level of surface temperature, the influence of precipitations becomes more important.

The example of retarded cooling of the strand surface in the center of an oscillation mark realized by the reduction of the heat flux in the mold by 20 and 30 pct, illustrates the importance of the initial cooling for the final austenite grain size. These simplified assumptions lead to an increase of the final austenite grain size by more than 40 pct.

The presented prediction model proved to be a valuable tool for the simulation of grain growth under continuous-casting conditions. Further work will be addressed to consider other precipitations, such as (Ti, Nb)(C,N), and the validation for other conventional casting processes, namely, bloom and billet casting.

REFERENCES

1. K. Schwerdtfeger: *Crack Susceptibility of Steels in Continuous Casting and Hot Forming*, Verlag Stahleisen, Duesseldorf, Germany, 1994, pp. 13–24.
2. N.A. McPherson and A. McLean: *Continuous Casting Vol. 8: Transverse Cracking in Continuously Cast Products*, Iron and Steel Society, Warrendale, PA, 1997, pp. 49–73.
3. B. Mintz, S. Yue, and J.J. Jonas: *Int. Mater. Rev.*, 1991, vol. 36 (5), pp. 187–217.
4. Y. Maehara, H. Tomono, and K. Yasumoto: *Trans. ISIJ*, 1987, vol. 27, pp. 103–09.
5. P. Deprez, J.P. Bricout, and J. Oudin: *Mater. Sci. Eng.*, 1993, vol. A168, pp. 17–22.
6. M. Suzuki, H. Hayashi, H. Shibata, T. Emi, and I.-J. Lee: *Steel Res.*, 1999, vol. 70 (10), pp. 412–19.
7. D.N. Crowther and B. Mintz: *Mater. Sci. Technol.*, 1986, vol. 2, pp. 951–55.
8. D.N. Crowther and B. Mintz: *Mater. Sci. Technol.*, 1986, vol. 2, pp. 1099–1105.
9. T. Emi: *The Making, Shaping and Treating of Steel*, 11th ed., Casting Volume, *Surface Defects on Continuously Cast Slabs*, AISI Steel Foundation, Pittsburgh, PA, 2003, pp. 20–58.
10. S. Harada, S. Tanaka, H. Misuri, S. Mizoguchi, and H. Horiguchi: *ISIJ Int.*, 1990, vol. 30 (4), pp. 310–16.
11. C. Bernhard, R. Pierer, A. Tubikanec, and C. Chimani: *Continuous-Casting and Hot-Rolling Conf. CCR'04, Proceedings of the Continuous-Casting and Hot-Rolling Conf.*, Linz, Austria, 2004, Paper No. 6.3, pp. 1–9.
12. C. Ouchi and K. Matsumoto: *Trans. ISIJ*, 1982, vol. 22, pp. 181–89.
13. B. Mintz, A. Crowley, R. Abushosha, and D.N. Crowther: *Mater. Sci. Technol.*, 1999, vol. 15, pp. 1179–85.
14. B. Mintz, R. Abushosha, and A. Cowley: *Mater. Sci. Technol.*, 1998, vol. 14, pp. 222–26.
15. Y. Ohmori and T. Kunitake: *Met. Sci.*, 1983, vol. 17, pp. 325–32.
16. Y. Maehara, K. Yasumoto, H. Tomono, T. Nagamichi, and Y. Ohmori: *Mater. Sci. Technol.*, 1990, vol. 6, pp. 793–805.
17. K. Yasumoto, T. Nagamichi, Y. Maehara, and K. Gunji: *Tetsu-to-Hagané (J. Iron Steel Inst. Jpn.)*, 1987, vol. 73 (14), pp. 1738–45.
18. J. Miettinen, S. Louhenkilpi, and L. Holappa: *ISIJ Int.*, 1996, vol. 36, pp. 183–86.
19. K. Schwerdtfeger, A. Köthe, J.M. Rodriguez, and W. Bleck: *Thin Slab Casting*, EUR 19409/1 EN, Luxembourg, 2001, vol. 1, pp. 33–48.
20. I. Andersen and O. Grong: *Acta Metall. Mater.*, 1995, vol. 43 (7), pp. 2673–88.
21. B. Dutta and C.M. Sellars: *Mater. Sci. Technol.*, 1987, vol. 3, pp. 197–206.
22. B. Weisgerber, K. Harste, and W. Bleck: *Steel Res. Int.*, 2004, vol. 75 (10), pp. 686–92.
23. R. Dippenaar, S.-C. Moon, and E.S. Szekeres: *Iron & Steel Technology Conf. Proceedings, AISTech 2006*, Publication of the

Association for Iron & Steel Technology, Cleveland, OH, 2006, pp. 833–44.
24. A.A. Howe: *Segregation and Phase Distribution During Solidification of Carbon, Alloy and Stainless Steels*, EUR 13302, ECSC, Luxembourg, 1991, pp. 31–40.
25. J. Reiter, C. Bernhard, and H. Preßlinger: *Materials Science and Technology*, MS&T '06, Conf. Exhib., Cincinnati, OH, Oct. 2006, pp. 805–16.
26. A.K. Giumelli, M. Militzer, and E.B. Hawbold: *ISIJ Int*., 1999, vol. 39 (3), pp. 271–80.
27. H. Hiebler and C. Bernhard: *Steel Res*., 1999, vol. 69 (8–9), pp. 349–55.
28. C. Bernhard, H. Hiebler, and M. Wolf: *Rev. Métall., Cahiers d'Information Techn*., 2000, vol. 97 (3), pp. 333–44.
29. C. Bernhard and G. Xia: *Ironmaking and Steelmaking*, 2006, vol. 33 (1), pp. 52–56.
30. C. Bernhard, H. Moitzi, H. Hiebler, and M. Wolf: *Conference: Modeling of Casting, Welding and Advanced Solidification Processes VIII*, San Diego, CA, June 1998, pp. 923–30.
31. C.S. Smith: *American Institute of Mining and Metallurgical Engineers*, American Institute of Mining and Metallurgical Engineers Inc., Technical Publication No. 2387, 1948, vol. 175, pp. 1–37.
32. H. Hu and B.B. Rath: *Met. Trans*., 1970, vol. 1 (11), pp. 3181–84.
33. M. Militzer, A. Giumelli, E.B. Hawbolt, and T.R. Meadowcroft: *Metall. Mater. Trans. A*, 1996, vol. 27A, pp. 3399–3409.
34. S. Uhm, J. Moon, C. Lee, J. Yoon, and B. Lee: *ISIJ Int*., 2004, vol. 44 (7), pp. 1230–37.
35. T. Maruyama, M. Kudoh, and Y. Itoh: *Tetsu-to-Hagané*, 2000, vol. 86 (2), pp. 86–91.
36. E.T. Turkdogan: *Iron Steelmaker*, 1989, vol. 16 (5), pp. 61–75.
37. E.G. Wilson and T. Gladman: *Int. Mater. Rev*., 1988, vol. 33 (5), pp. 221–86.
38. C. Bernhard and T. Sjökvist: *Berg. Huettenm. Mon*., 2006, vol. 151 (5), pp. 189–95.
39. H. Resch: Master's thesis, University of Leoben, Austria, 1998.
40. E. Takeuchi and J.K. Brimacombe: *Metall. Mater. Trans. B*, 1985, vol. 16B, pp. 605–24.